Mutations that prevent phosphorylation of the BMP4 prodomain impair proteolytic maturation of homodimers leading to early lethality in mice

Hyung-seok Kim[1§] Mary Sanchez[1§†], Joshua Silva[1§¶], Heidi L. Schubert[3], Rebecca Dennis[1], Christopher P. Hill[3], Jan L. Christian[1,2*]

[1]Department of Neurobiology
[2]Internal Medicine, Division of Hematology and Hematologic Malignancies
[3]Department of Biochemistry
University of Utah
20 North 1900 East
Salt Lake City, Utah 84132-3401

[§]These authors contributed equally to this work.

[*]To whom correspondence should be addressed:
Email: jan.christian@neuro.utah.edu

[†] Environmental Life Sciences
Arizona State University
Tempe, AZ 85281

[¶] Cell and Molecular Biology
Duke University
Durham, NC 27710

Running title

BMP4 prodomain mutant mice

Keywords

BMP4, prodomain, human mutations, FAM20C, *Xenopus,* mouse

Abstract

Bone morphogenetic protein4 (BMP4) plays numerous roles during embryogenesis and can signal either as a homodimer, or as a more active BMP4/7 heterodimer. BMPs are generated as inactive precursor proteins that dimerize and are cleaved to generate the bioactive ligand and inactive prodomain fragments. In humans, heterozygous mutations within the prodomain of BMP4 are associated with birth defects. We studied the effect of two of these mutations (p.S91C and p.E93G), which disrupt a conserved FAM20C phosphorylation motif, on ligand activity. We compared the activity of BMP4 homodimers or heterodimers generated from BMP4, BMP4^{S91C} or BMP4^{E93G} precursor proteins in *Xenopus* embryos and found that these mutations reduce the activity of BMP4 homodimers but not heterodimers. We generated *Bmp4*^{S91C} and *Bmp4*^{E93G} knock-in mice and found that *Bmp4*$^{S91C/S91C}$ mice die by E11.5 and display reduced BMP activity in multiple tissues including the heart at E10.5. Most *Bmp4*$^{E93G/E93G}$ mice die before weaning and *Bmp4*$^{-/E93G}$ mutants die prenatally with reduced or absent eyes, heart and ventral body wall closure defects. Mouse embryonic fibroblasts (MEFs) isolated from *Bmp4*^{S91C} and *Bmp4*^{E93G} embryos show accumulation of BMP4 precursor protein, reduced levels of cleaved BMP ligand and reduced BMP activity relative to MEFs from wild type littermates. Because *Bmp7* is not expressed in MEFs, the accumulation of unprocessed BMP4 precursor protein in mice carrying these mutations most likely reflects an inability to cleave BMP4 homodimers, leading to reduced levels of cleaved ligand and BMP activity in vivo. Our results suggest that phosphorylation of the BMP4 prodomain is required for proteolytic activation of BMP4 homodimers, but not heterodimers.

Summary Statement

Mutations associated with birth defects in humans that prevent phosphorylation of the BMP4 prodomain preclude proteolytic activation of the precursor protein

Introduction

BMPs are secreted molecules that were initially discovered as bone inducing factors and were subsequently shown to play numerous roles during embryogenesis (Bragdon et al., 2011). *Bmp2, 4, 5, 6* and *7* are broadly expressed throughout embryogenesis, often in overlapping patterns (Danesh et al., 2009). *Bmp2* and *Bmp4* play important and non-redundant developmental roles, as mice homozygous for null mutations in either gene null die during early development (Winnier et al., 1995; Zhang and Bradley, 1996). Although *Bmp5, Bmp6 or Bmp7* null homozygotes survive until birth or beyond, *Bmp5;Bmp7* and *Bmp6;Bmp7* double mutants die during embryogenesis, revealing functional redundancy within this subgroup (Kim et al., 2001; Solloway and Robertson, 1999).

BMPs are grouped into subfamilies based on sequence similarity and can signal as either homodimers or as heterodimers. The class I BMPs, BMP2 and BMP4, can heterodimerize with class II BMPs, consisting of BMPs 5-8 (Guo and Wu, 2012). Heterodimers composed of class I and class II BMPs show a higher specific activity than homodimers. For example, BMP2/7, BMP4/7 and BMP2/6 heterodimers are significantly more potent than any homodimer in multiple assays (Aono et al., 1995; Chauhan et al., 2024; Kaito et al., 2018; Valera et al., 2010). In vivo, endogenous Bmp2/7 heterodimers are essential to establish the dorsoventral axis in fish (Little and Mullins, 2009) and *Drosophila* (Shimmi et al., 2005). More recent studies have shown that endogenous BMP4/BMP7 and BMP2/7 heterodimers are required to generate full BMP activity in most or all tissues of mouse embryos (Kim et al., 2019).

The choice of whether a given BMP will form a homodimer or a heterodimer is made within the biosynthetic pathway. BMPs are made as inactive precursor proteins that dimerize and fold within the endoplasmic reticulum (ER) and are cleaved by members of the proprotein convertase (PC) family, such as furin, to generate the active, disulfide-bonded ligand and two prodomain monomers (Bragdon et al., 2011). Prodomains lack canonical signaling activity but are essential for ligand folding and dimerization, and can regulate subcellular trafficking, localization and

bioavailability of mature ligands (Constam, 2014; Cui et al., 2001; Goldman et al., 2006; Gray and Mason, 1990; Harrison et al., 2011; Sengle et al., 2008; Tilak et al., 2014). Structural studies show that some dimerized TGF-β superfamily precursors adopt a conformation whereby the prodomain of one monomer contacts the ligand domain of the opposite monomer (Wang et al., 2016; Zhao et al., 2018), suggesting that prodomains may play a key role in heterodimer formation and function.

Bmp4 and Bmp7 preferentially form heterodimers rather than either homodimer when co-expressed in *Xenopus,* and the Bmp4 prodomain is necessary and sufficient to generate properly folded, functional BMP4 homodimers and Bmp4/7 heterodimers (Neugebauer et al., 2015). Bmp4 is sequentially cleaved at two sites within the prodomain to generate an active ligand (Cui et al., 2001). An initial cleavage occurs adjacent to the ligand domain, and this generates a non-covalently associated prodomain/ligand complex that is subsequently dissociated by cleavage at an upstream site (Figure 1A) (Degnin et al., 2004). Sequential cleavage at both sites, and formation of the transient prodomain/ligand complex is essential to generate a stable, fully active ligand (Goldman et al., 2006; Tilak et al., 2014). By contrast, BMP7 is cleaved at a single site and the prodomains remain transiently and noncovalently associated with the ligand following cleavage. The Type II BMP receptor then competes with the N-terminus of the prodomain for ligand binding and displaces the prodomain from the complex to allow for downstream signaling (Sengle et al., 2008). The same may be true for Bmp4/7 heterodimers, since both prodomains remain non-covalently attached following cleavage (Figure 1B) (Neugebauer et al., 2015).The factors that drive formation of fully functional heterodimers or homodimers are unknown.

In humans, heterozygous mutations within the prodomain of *BMP4* are associated with a spectrum of ocular, brain, kidney, dental and palate abnormalities (Bakrania et al., 2008; Chen et al., 2007; Nixon et al., 2019; Reis et al., 2011; Schild et al., 2013; Suzuki et al., 2009; Weber et al., 2008; Yu et al., 2019; Zhang et al., 2009). Two of the BMP4 prodomain missense mutations found in humans (c.271A >T, p.S91C and c.278A>G, p.E93G) disrupt a highly conserved

phosphorylation motif (S-X-E/pS) (Figure 1C) that is recognized by the secretory pathway kinase Family with sequence similarity to 20C (FAM20C). FAM20C phosphorylates endogenous BMP4 at S91 within this motif (Tagliabracci et al., 2015) and BMP activity is decreased in ameloblasts and dental epithelium from *Fam20c* mutant mice (Liu et al., 2018; Liu et al., 2020). Mutations in human *FAM20C* cause the often-lethal disorder, Raine syndrome (Simpson et al., 2007). Some of the dental and bone defects observed in Raine patients can be accounted for by loss of phosphorylation of FAM20C substrates involved in biomineralization (Faundes et al., 2014) and of FGF23 (Tagliabracci et al., 2014). The etiology of other defects in these patients, such as cleft palate and craniofacial abnormalities, is unclear. Whether and how phosphorylation of the prodomain impacts BMP ligand formation or activity is unknown.

In the current studies, we analyzed the impact of p.S91C and p.E93G prodomain mutations on ligand function. We found that these mutations disrupt the formation of functional BMP4 homodimers, but not BMP4/7 heterodimers in ectopic expression assays. Mice carrying $Bmp4^{S91C}$ or $Bmp4^{E93G}$ knock in mutations show early lethality, reduced BMP activity and accumulation of uncleaved homodimeric BMP4 precursor proteins with a concomitant loss of cleaved ligand. Our results suggest that phosphorylation of the BMP4 prodomain is required for proteolytic activation of BMP4 homodimers, but not heterodimers.

Results

Point mutations predicted to interfere with phosphorylation of the BMP4 prodomain selectively interfere with BMP4 homodimer but not BMP4/7 heterodimer activity.

Humans heterozygous for missense mutations p.S91C or p.E93G within the BMP4 prodomain (Figure 1A,C) display enhanced predisposition to colorectal cancer, micropthalmia, skeletal defects, brain abnormalities, cleft lip and/or kidney dysgenesis (Bakrania et al., 2008; Lubbe et al., 2011; Suzuki et al., 2009; Weber et al., 2008), suggesting that these prodomain mutations interfere with the activity of BMP4 homodimers or BMP4/7 heterodimers. To test this possibility,

we injected RNA encoding murine BMP4^{HAMyc}, BMP4^{HAMycS91C} or BMP4^{HAMycE93G} into *Xenopus* embryos near the dorsal marginal zone (DMZ) of four cell embryos. We have previously shown that these epitope tags do not interfere with the activity of BMP4 in vivo (Tilak et al., 2014). The DMZ was explanted from embryos at the early gastrula stage and immunoblots of DMZ extracts were probed for phosphoSmad1,5,8 (hereafter shortened to pSmad1), which provides a direct read out for BMP activity (assay illustrated in Figure 1D). Levels of pSmad1 are high in the VMZ, where endogenous Bmp ligands are expressed, but low in the DMZ, where BMP inhibitors are expressed. Ectopic BMP4^{S91C} or BMP4^{E93G} induced significantly less pSmad1 than did wild type BMP4 (Figure 1D, E), demonstrating that these point mutations interfere with BMP4 homodimer activity. We also tested whether a putative phosphomimetic mutant (BMP4^{S91D}) would interfere with ligand activity. pSmad1 activity was lower in DMZ explants expressing BMP4^{S91D} than in those expressing wild type BMP4 but was significantly higher than in those expressing BMP4^{S91C} (Fig. S1A, B). We used a second ectopic expression assay to verify results. RNA encoding wild type or mutant BMP4 was injected near the animal pole of 2-cell *Xenopus* embryos, ectoderm was explanted at the early gastrula stage and expression of the BMP target gene, *tbxt,* was analyzed by semi-quantitative (semi-q) RT-PCR. *tbxt* levels were significantly lower in explants from embryos expressing BMP4^{S91C} or BMP4^{E93G} relative to those expressing wild type BMP4 (Fig. 1G, H). These findings suggest that phosphorylation of S91 is required to generate fully active BMP4 homodimers.

We then repeated these assays in embryos co-injected with RNA encoding wild type or mutant BMP4 together with BMP7. We have previously shown that BMP4 and BMP7 preferentially generate heterodimers over either homodimer when co-expressed and that heterodimers generate significantly more BMP activity than either homodimer (Neugebauer et al., 2015). There was no significant difference in the levels of pSmad1 (Fig. 1D, F) or *tbxt* (Fig. 1G, I) induced in embryos co-injected with BMP7 together with wild type or either point mutant form of BMP4. This

suggests that the S91C and E93G prodomain point mutations selectively interfere with BMP4 homodimer but not BMP4/7 heterodimer activity.

Bmp4^{S91C} homozygotes die during mid-embryogenesis and show reduced BMP activity in multiple tissues

To ask whether S91C and E93G prodomain missense mutations interfere with endogenous BMP4 activity in vivo, we introduced nucleotide mutations to encode single amino acid changes (p.S91C or p.E93G) along with sequence encoding an HA epitope tag into the prodomain of the *Bmp4* allele in mice (*Bmp4^{S91C}* and *Bmp4^{E93G}*). We have previously generated control mice that carry an HA-epitope tag at the same position in the wild type *Bmp4* locus, as well as a myc tag in the ligand domain (*Bmp4^{HAMyc}*). These mice are adult viable and show no visible defects (Tilak et al., 2014).

Bmp4$^{S91/+}$ mice were intercrossed to determine whether homozygotes were adult viable. *Bmp4^{S91C}* homozygotes were not recovered at weaning (Table 1A). We then established timed matings to determine when during embryogenesis death occurred. *Bmp4$^{S91C/S91C}$* mutants were recovered at the predicted Mendelian frequency at embryonic day (E)9.5 and E10.5 (Table 2A, Table S1C, D) but were slightly smaller than littermates at E10.5 (Fig. 2A-C) and were absent or resorbing by E11.5 (Fig. 2D-F, Table 2A, Table S1A, B).

To determine whether and where BMP activity is reduced in *Bmp4^{S91C}* homozygotes, we analyzed BMP activity in *BRE*:*LacZ* transgenic embryos at E10.5. This transgene contains a BMP-responsive element coupled to LacZ, which serves as an in vivo reporter of BMP signaling downstream of all endogenous BMP ligands (Monteiro et al., 2004). X-GAL staining of *Bmp4$^{+/+}$;BRE:LacZ* embryos revealed strong endogenous BMP activity in the brain and spinal cord, eye, branchial arches (BA), limb buds, heart, somitic mesoderm (SM) and ventroposterior mesoderm (VPM) (Fig. 2G, J). *Bmp4$^{S91C/S91C}$;BRE:LacZ* mutants were smaller and exhibited a severe (Fig. 2H, K, 1 out of 6 embryos) or modest (Fig. 2I,L; 5 out of 6 embryos) reduction in BMP

activity in all tissues except the eye. Notably, LacZ staining was also reduced in the heart and VPM of *Bmp4*$^{S91C/S91C}$*;BRE:LacZ* embryos relative to wild type littermates at E9.5 (Fig. S2).

We also examined expression of the BMP target gene *Nkx2-5* in the heart of wild type and *Bmp4*^{S91C} mutant littermates using whole mount in situ hybridization. At E10.5 expression of Nkx2-5 was reduced (1/3) or nearly absent (2/3) in hearts of *Bmp4*$^{S91C/S91C}$ embryos relative to littermates (Fig. 2M-O). Although mutant hearts were smaller than littermates, they showed grossly normal patterning of atria, ventricles and outflow tract (Fig. 2M-O).

Bmp4$^{E93G/E93G}$ female mice are underrepresented at weaning and _Bmp4_$^{-/E93G}$ mutants die during late gestation with defects in ventral body wall closure, small eyes and heart defects.

Bmp4$^{E93/+}$ mice were intercrossed to determine viability. *Bmp4*^{E93G} homozygotes were underrepresented at weaning, and this could be entirely accounted for by an underrepresentation of female but not male *Bmp4*$^{E93G/E93G}$ mice (Table 1B). *Bmp4*$^{E93G/E93G}$ male mice appeared grossly normal at weaning, although they weighed slightly less than wild type littermates (Fig. S3A). Unilateral or bilateral microphthalmia, anopthalmia and/or craniofacial defects were observed with low frequency in *Bmp4*^{E93G} heterozygotes at late gestation (Fig. S3B-D) (*n*=1/12) or at weaning (*n*=6/74). These defects have been previously reported in *Bmp4* hypomorphic mice (Bonilla-Claudio et al., 2012; Furuta and Hogan, 1998; Goldman et al., 2006) and in humans heterozygous for the *BMP4*^{E93} prodomain mutation (Bakrania et al., 2008).

To ask whether a single allele of *Bmp4*^{E93G} is sufficient to support viability, we intercrossed mice heterozygous for a null allele of *Bmp4* (*Bmp4*$^{-/+}$) with *Bmp4*^{E93G} heterozygotes. *Bmp4*$^{-/E93G}$ compound mutants were not recovered at weaning (Table 1C) but were recovered at the predicted Mendelian frequency through E14.5 (Table 2B, Table S2). At E13.5-14.5, all *Bmp4*$^{-/E93G}$ mutants were slightly runted relative to littermates and had defects in ventral body wall closure in which the liver was partially or fully externalized (*n*=16/16) (Fig. 3A-G). Most *Bmp4*$^{-/E93G}$ embryos also had small or absent eyes (*n*= 15/16) (Fig. 3C, G). A subset of mice heterozygous for the null allele of

Bmp4 also had small or absent eyes (2/19) as previously reported (Dunn et al., 1997). Histological examination of hearts dissected from $Bmp4^{-/E93G}$ mutants at E14.5 revealed highly trabeculated ventricular walls that failed to undergo compaction (3/3) and ventricular septal defects (2/3) (VSDs) (Fig. 3I) that were never observed in wild type embryos (Fig. 3H). A similar spectrum of abnormalities including small or absent eyes, failure to close the ventral body wall and VSDs have previously been reported in mice with reduced dosage of *Bmp4* (Furuta and Hogan, 1998; Goldman et al., 2009; Kim et al., 2019; Uchimura et al., 2009).

$Bmp4^{S91C/E93G}$ female compound heterozygotes are underrepresented at weaning

$Bmp4^{S91/+}$ and $Bmp4^{E93G/+}$ mice were intercrossed to determine whether compound heterozygotes were adult viable. $Bmp4^{S91C/E93G}$ mice were underrepresented at weaning, and this could be entirely accounted for by an underrepresentation of female but not male compound mutants (Table 1D). $Bmp4^{S91C/E93G}$ mice appeared grossly normal at weaning, although they weighed slightly, but not significantly, less than littermates (Fig. S4). The late lethality of female, but not male $Bmp4^{S91C/E93G}$ compound heterozygotes and $Bmp4^{E93G}$ homozygotes, along with their grossly normal phenotype contrasts with the early (E11) lethality and more severe phenotypic defects of $Bmp4^{S91C}$ homozygotes. These results raise the possibility that loss of FAM20C-mediated phosphorylation of the BMP4 prodomain fully accounts for the late lethality of $Bmp4^{E93G/E93G}$ and $Bmp4^{S91C/E93G}$ mutants whereas the p.S91C mutation may cause additional, FAM20C-independent defects in BMP4 function when encoded on both alleles of *Bmp4.*

E93G and S91C mutations lead to accumulation of BMP4 precursor protein and reduced levels of cleaved ligand and pSmad1 in vivo

To ask if BMP activity and/or protein levels are reduced in $Bmp4^{S91C}$ or $Bmp4^{E93G}$ mutants, we used immunoblot analysis to compare levels of pSMAD1 and BMP4 in E10.5 embryonic lysates isolated from wild type or mutant littermates. Levels of BMP4 precursor protein were significantly

higher, and levels of pSMAD1 and of cleaved BMP4 ligand were significantly lower in E10.5 lysates from *Bmp4*^{S91C} homozygotes compared to wild type controls (Fig. 4A-D). No significant differences in levels of pSMAD1, BMP4 precursor or BMP4 ligand were observed in E10.5 lysates from *Bmp4*^{E93G} mutants compared to wild type controls (Fig. 4E-H), or in wild type embryos carrying HA and Myc epitope tags compared to untagged controls (Fig. S5A-D). When we repeated this analysis in E13.5 mouse embryonic fibroblasts (MEFs) isolated from wild type or mutant littermates, we found that pSMAD1 levels were significantly reduced in *Bmp4*^{S91C} heterozygotes (Fig. 4I, J) and in *Bmp4*^{E93G} homozygotes (Fig. 4M, N) compared to wild type controls. In addition, levels of BMP4 precursor protein were increased and levels of cleaved ligand were reduced in *Bmp4*^{S91C} heterozygotes (Fig. 4I, K, L) and in *Bmp4*^{E93G} heterozygotes or homozygotes (Fig. 4M, O, P) compared to wild type controls. Thus, p.E93G and p.S91C mutations in the prodomain of BMP4 interfere with proteolytic maturation of the BMP4 precursor, leading to accumulation of unprocessed precursor protein and reduced levels of cleaved ligand and BMP activity in vivo.

BMP4^{E93G} *and BMP4*^{S91C} *precursor proteins are O-glycosylated and exit the ER*

FAM20C-mediated phosphorylation of FGF23, like that of BMP4, is required for furin mediated cleavage (Wang et al., 2012). Mechanistically, phosphorylation of FGF23 prevents *O*-glycosylation of a nearby residue, and *O*-glycosylation sterically blocks the furin cleavage site (Tagliabracci et al., 2014). To test if a similar mechanism accounts for lack of cleavage of BMP4^{E93G} or BMP4^{S91C}, MEFS from E13.5 wild type, *Bmp4*$^{E93G/E93G}$ or *Bmp4*$^{S91C/+}$ mice were incubated in the presence or absence of O-Glycosidase and Neuraminidase and BMP4 precursor protein was analyzed on immunoblots. Treatment with these deglycosylases led to a more rapid migration of the BMP4 precursor protein, indicating that BMP4 is *O*-glycosylated, but there was no difference in the migration of wild type or point mutation precursors in the presence or absence of deglycosylases (Fig. 5A), suggesting that phosphorylation does not alter O-glycosylation.

Another mechanism by which FAM20C-mediated phosphorylation might regulate cleavage of the BMP4 is if it is required for the BMP4 precursor protein to adopt its native folded conformation so that it is able to exit the ER. We analyzed N-linked glycosylation of endogenous wild type and mutant precursor proteins present in cultured MEFs. N-linked carbohydrate residues that are transferred onto proteins in the ER are sensitive to digestion with Endoglycosidase H (Endo H), but when further modified in the Golgi they become Endo H resistant but remain sensitive to digestion with Peptide N-Glycosidase F (PNGase). Thus, Endo H resistance/PNGase sensitivity is a hallmark of proteins that are properly folded and able to traffic from the ER into the Golgi. As shown in Figure 5B, Endo H sensitive (asterisks) and Endo H resistant/PNGase F sensitive (arrowheads) forms of wild type and mutant precursors were detected in MEFs. We have previously shown that high mannose, Endo H sensitive carbohydrates are retained at one or more glycosylation site(s) on BMP4 ligand homodimers even after BMP4 has folded, trafficked through the trans-Golgi network (TGN) and been cleaved (Degnin et al., 2004). This explains why partial EndoH sensitivity is observed in both wild type and mutant precursors that have exited the ER. Collectively, our findings are most consistent with a model in which FAM20C-mediated phosphorylation of the BMP4 prodomain is not required for folding or exit of the precursor protein from the ER, but is required for PC recognition and/or for trafficking to post-TGN compartment(s) where BMP4 is cleaved (Tilak et al., 2014).

Discussion

Humans heterozygous for p.S91C or p.E93G point mutations within the prodomain of BMP4 show congenital birth defects and/or enhanced predisposition to colorectal cancer (Bakrania et al., 2008; Lubbe et al., 2011; Suzuki et al., 2009; Weber et al., 2008). These mutations disrupt a conserved -S-X-E- motif required for FAM20C-mediated phosphorylation of Ser91 suggesting that phosphorylation of the prodomain, which itself lacks biologic activity, is required for ligand activity. Here we show that these mutations lead to reduced activity of BMP4 homodimers but not BMP4/7

heterodimers in *Xenopus* assays. Furthermore, in mice carrying either of these mutations proteolytic maturation of endogenous BMP4 is impaired, leading to reduced BMP activity. Our results suggest that phosphorylation of the BMP4 prodomain by FAM20C is essential for furin to cleave the precursor protein to generate active BMP4 homodimers.

How might phosphorylation facilitate proteolytic maturation of BMP4 homodimers? We have previously shown that cleavage of BMP4 occurs in membrane proximal vesicles, and this is proposed to protect the ligand from degradation by passing it off to extracellular matrix binding partners as cleavage occurs (Tilak et al., 2014). This raises the question of how BMP4 can traffic through the TGN, where furin is first active (Anderson et al., 2002; Thomas, 2002), yet escape cleavage until it reaches the cell surface. We propose two possible mechanisms by which FAM20C-mediated phosphorylation facilitates cleavage of BMP4 and also ensures that this occurs in a membrane proximal subcellular compartment. One model proposes that phosphorylation occurs in the TGN and directs trafficking of BMP4 out of the golgi to the cell surface via a route that is distinct from the pathway taken by furin (Thomas, 2002) (Fig. 6A). In this model, furin would first encounter and cleave BMP4 in membrane-proximal intracellular compartments, similar to what has been observed for other substrates (Thomas, 2002). This model predicts that BMP4^{E93G} and BMP4^{S91C} precursor proteins are trapped in the TGN or other subcellular compartments that furin cannot access. An alternate model proposes that furin, BMP4 and FAM20C traffic together out of the TGN but that the kinase is not active until it exits the TGN. In this model, phosphorylation in a membrane proximal compartment is required for furin to cleave BMP4 (Fig. 6B). In support of this model, FAM20C is synthesized as a basally active kinase that is tethered to the golgi by its propeptide. Propeptide cleavage releases Fam20C from the Golgi, and greatly enhances its kinase activity as it to traffics to the cell surface (Chen et al., 2021). Furthermore, AlphaFold structure predictions position the phosphorylated serine of BMP4 (Ser91) in close proximity to the -R^{287}-R-R-A-K-R^{292} sequence motif recognized by furin (Fig. 6C-E) (Jumper et al., 2021; Varadi and Velankar, 2023), consistent with the possibility that

phosphorylation is required for furin to access the cleavage site. This model predicts that BMP4^{E93G} and BMP4^{S91C} precursor proteins can traffic to membrane proximal locations but remain uncleaved.

Our results suggest that phosphorylation of the BMP4 prodomain is required for cleavage of BMP4 homodimers, but not BMP4/7 heterodimers. Interestingly, alphafold predicts that the furin cleavage motif on each monomeric chain of BMP4 homodimers (Figure 6F, purple) is situated on opposite sides of the dimeric molecule, each in close proximity to S91 (Fig. 6C, D). By contrast, the two furin cleavage motifs (Fig. 6G, purple) on heterodimers composed BMP4 (light shading) and BMP7 (dark shading) are predicted to be located on the same face of the dimeric molecule, in close proximity to each other (Jumper et al., 2021; Varadi and Velankar, 2023). This raises the possibility that furin can be recruited to the cleavage motif on BMP7, enabling it to access the cleavage motif on BMP4 independent of phosphorylation when present as a BMP4/7 heterodimer.

The late-stage lethality of *Bmp4*$^{E93G/E93G}$ and *Bmp4*$^{S91C/E93G}$ mice is consistent with a selective loss of BMP4 homodimers rather than BMP4/7 heterodimers since mice homozygous for a mutation (*Bmp7*$^{R\text{-}GFlag}$) that disrupts the formation of functional BMP2/7 and BMP4/7 heterodimers, or mice compound heterozygous for the *Bmp7*$^{R\text{-}GFlag}$ and *Bmp4* null alleles die by E11.5 (Kim et al., 2019). Furthermore, whereas *Bmp7*$^{R\text{-}GFlag/R\text{-}GFlag}$ and *Bmp7*$^{R\text{-}GFlag/+}$;*Bmp4*$^{-/+}$ mutants show stereotypical heart defects including thinner myocardial walls, a common atrium, and a small, malformed OFT relative to wild type littermates, *Bmp4*$^{S91C/S91C}$ mutant hearts show grossly normal patterning of atria, ventricles and outflow tract while *Bmp4*$^{-/E93G}$ mutant hearts show reduced myocardial trabeculation and VSDs. The latter heart defects phenocopy those observed in *Ngly1* mutant mice, which also show VSDs, poorly elaborated myocardial trabeculation and late stage (P0) lethality (Fujihira et al., 2017; Galeone et al., 2020). NGLY1 is a deglycosylase that is required to clear misfolded BMP4 precursor monomers from the ER. This, in turn, promotes the formation of properly folded BMP4 homodimers that can be transported out of the ER to be cleaved to generate the functional ligand (Galeone et al., 2020). The *Drosophila* ortholog of

NGLY1 (Pngl1) is required for formation of functional Dpp (the fly ortholog of BMP2/4) homodimers, but not heterodimers (Galeone et al., 2017). In *pngl1* mutant flies, and in MEFs from *Ngly1* mutant mice, Dpp/BMP4 precursor accumulates in the ER and very little cleaved ligand is observed (Galeone et al., 2020). By contrast, in *Bmp4*$^{E93G/E93G}$ mutant MEFs BMP4 precursor accumulates in post-ER compartments but very little cleaved ligand is observed. The almost complete loss of mature BMP4 secreted from *Bmp4*$^{E93G/E93G}$ mutant MEFs is consistent with a selective loss of homodimers since *Bmp7* is not expressed in MEFs (Lienert et al., 2011) and thus BMP4 is predicted to exist primarily as a homodimer in these cells. Thus, mutations that prevent phosphorylation of the BMP4 prodomain, or mutations in *Ngly1* both lead to reduced levels of mature BMP4 homodimers and similar phenotypic consequences, although the mechanisms underlying the loss of proteolytic maturation are distinct.

Our findings demonstrate that *Bmp4*^{S91C} and *Bmp4*^{E93G} are hypomorphic alleles, although *Bmp4*^{S91C} causes a more severe loss of function. Although both mutations are predicted to prevent FAM20C mediated phosphorylation of the BMP4 prodomain, it is likely that the p.S91C mutation leads to additional defects in protein function due to deleterious effects of introducing an ectopic cysteine residue. BMP4 folds into a cystine knot containing three stereotypical intermolecular disulfide bonds that stabilize ligand monomers and a single intramolecular disulfide bond that stabilizes the dimer (Schwarz, 2017). The addition of an ectopic cysteine residue may lead to aberrant intramolecular or intermolecular disulfide bonds in precursor proteins, as suggested by biochemical analysis of BMP4^{S91C} homodimers expressed in cultured mammalian cells (Tabatabaeifar et al., 2009). This interpretation is consistent with our finding that *Bmp4*$^{S91C/E93G}$ compound heterozygotes have a less severe phenotype than *Bmp4*$^{S91C/S91C}$ mice, and with our observation that ectopically expressed BMP4^{S91D} generates significantly higher activity in *Xenopus* embryos than does BMP4^{S91C}.

In summary, our data suggest that phosphorylation of the BMP4 prodomain is required for proteolytic maturation of BMP4 homodimers but not heterodimers, although further studies will be

required to validate this in vivo and to understand the process mechanistically. Previous studies have demonstrated the importance of BMP heterodimers as endogenous ligands in multiple organisms (Bauer et al., 2023; Kim et al., 2019; Little and Mullins, 2009; Shimmi et al., 2005). The current findings show that BMP4 homodimers are also functionally relevant. The existence and relative role of heterodimers versus homodimers is likely to vary widely among different organisms, tissues and developmental stages. Additional studies are required to understand where and how a given BMP is directed to form one species of the other in vivo.

Materials and Methods

Xenopus embryo culture and manipulation

Animal procedures followed protocols approved by the University of Utah Institutional Animal Care and Use Committee. Embryos were obtained, microinjected, and cultured as described (Mimoto and Christian, 2011). Embryo explants were performed as described (Mimoto et al., 2015; Neugebauer et al., 2015).

Mouse strains

Animal procedures followed protocols approved by the University of Utah Institutional Animal Care and Use Committees. *Bmp4*$^{LacZ/+}$and BRE-LacZ mice were obtained from Dr. B. Hogan (Duke University) and Dr. C. Mummery (Leiden University), respectively. *Bmp4*^{S91C} *and Bmp4*^{E93G} mice were generated by personnel in the Mutation Generation & Detection and the Transgenic & Gene Targeting Mouse Core Facilities at the University of Utah using CRISPR-Cas9 technology. sgRNA RNAs (5'-TGAGCTCCTGCGGGACTTCG-3') were injected into C57BL/6J zygotes together with long single stranded donor DNA repair templates (E93G: 5'-GGAAGAAAAAAGTCGCCGAGATTCAGGGCCACGCGGGAGGACGCCGCTCAGGGCAGAGCCATG

AGCTCCTGCGGGACTTCGAaGCGACACTTTATCCATACGACGTGCCAGACTATGCACTACAGATGT TTGGGCTGCGCCGCCGTCCGCAGCCTAGCAAGAGCGCCGTCATTCCGGATTACATGAGGGATCT TTACCGGCTCCAGTCTGG**a**G**g**GGAGGAGGAGGAAGAGCAGAGCCAGGGAACCGGGCTTGAGTAC CCGGAGCGTCCCGCCAGCCGAGCCAACACTG-3'; S91C: 5'-GGAAGAAAAAAGTCGCCGAGATTCAGGGCCACGCGGGAGGACGCCGCTCAGGGCAGAGCCATG AGCTCCTGCGGGACTTCGAaGCGACACTTTATCCATACGACGTGCCAGACTATGCACTACAGATGT TTGGGCTGCGCCGCCGTCCGCAGCCTAGCAAGAGCGCCGTCATTCCGGATTACATGAGGGATCT TTACCGGCTCCAGT**g**TGG**c**GAGGAGGAGGAGGAAGAGCAGAGCCAGGGAACCGGGCTTGAGTAC CCGGAGCGTCCCGCCAGCCGAGCCAACACTG-3'; sequence encoding HA epitope underlined; nucleotide changes bold and small case) and Cas9 protein. G0 founders were crossed to C57BL/6J females to obtain heterozygotes. DNA fragments PCR-amplified from genomic DNA were sequenced to verify the presence of the epitope tag and absence of other sequence changes. Genotypes were determined by PCR amplification of tail DNA using primers that anneal to sequence immediately surrounding the HA epitope tag (5' primer: 5'-TATGCCAAGTCCTGCTAG-3' and 3' primer: 5'-GATCCCTCATGTAATCCG-3') under the following conditions: 94°C for 30 seconds, 60°C for 30 seconds, 72°C for 30 seconds, 35 cycles.

cDNA constructs

cDNAs encoding mouse $BMP4^{HAMyc}$ and $BMP7^{Flag}$ have been described previously (Kim et al., 2019; Tilak et al., 2014). cDNAs encoding $BMP4^{HAMycS91C}$, $BMP4^{HAMycS91D}$ and $BMP4^{HAMycE93G}$ were generated using a QuickChange II XL site-directed mutagenesis kit (Agilent Technologies).

Analysis of RNA

Total RNA was isolated using TRIzol (Invitrogen). Semi quantitative RT-PCR was performed as described (Nakayama et al., 1998) using an annealing temperature of 58°C.

In situ hybridization and ß-galactosidase staining

Embryos were processed for in situ hybridization with digoxigenin-labeled Nkx2.5 riboprobes as described previously (Wilkinson and Nieto, 1993). ß-galactosidase staining of BRE-LacZ embryos was performed as described (Lawson et al., 1999) and color was developed using RedGal. Investigators were blinded to genotype until after morphology and/or staining intensity had been documented.

Immunoblot analysis of *Xenopus* extracts Proteins were harvested from 10 pooled DMZ explants by freon extraction as described previously (Mimoto and Christian, 2011). Proteins were resolved by SDS-PAGE under reducing and non-reducing conditions and transferred onto PVDF membranes. Membranes were probed with anti-actin (1:10000, Sigma) and anti-pSmad1/5/8 (1:1000, Cell signaling) antibodies. Immunoreactive proteins were detected using Enhanced Chemiluminescence reagent (Pierce) and light emissions captured with x-ray film. Images were scanned and relative band intensity was quantified using ImageJ software.

Immunoblot analysis of mouse embryo lysates and MEFs

Mouse embryos were dissected from pregnant females at E10.5, homogenized in lysis buffer (150 mM NaCl, 20 mM Tris-Cl pH 7.5, 1mM EDTA, 1% Sodium deoxycholate, 1% NP40, 1X protease inhibitor (cOmplete Mini, EDTA-free, Roche), 1X phosphatase inhibitor cocktail (Sigma) and protein concentration was measured by BCA kit (Thermo Scientific). 80 ug, 10 ug and 5 ug of embryo lysates were used for detection of BMP4 mature ligand, BMP4 precursor and pSmad1, respectively. MEFs were isolated at E13.5 as described (Durkin et al., 2013) and cultured in 10% FBS, 1X pen/strep, 1x Glutamate in DMEM. Following the second passage, MEFs were cultured in serum containing media until they reached 80% confluency and were then cultured in serum free media for 24 hours before collecting cells and conditioned media. 800 ul of conditioned media

was used for TCA precipitation. Proteins were deglycosylated according to manufacturer's instructions using O-Glycosidase, Neuramidase, EndoH and PNGase purchased from NEB. Proteins were separated by electrophoresis on 10% or 12% gels and transferred to PVDF membranes that were probed with anti-Bmp4 (1:1000, Santa Cruz), anti-pSmad1/5 (1:1000, Cell Signaling) or anti-actin (1:10,000, Sigma) antibodies followed by HRP-conjugated anti-rabbit IgG or anti-mouse IgG2b (Jackson ImmunoResearch) secondary antibodies. Immunoreactive proteins were detected using Enhanced Chemiluminescence reagent (Pierce) and light emissions captured with x-ray film. Images were scanned and relative band intensity was quantified using ImageJ software.

Statistics

NIH Image J software was used to quantify band intensities. A student's *t*-test was used to compare differences in gene expression or protein levels between two groups. Differences with $P < 0.05$ were considered statistically significant. All results were reproduced in three biological replicates.

Acknowledgements

We thank Dr. Eyad Marashly for generating the BMP4^{E93G} cDNA and synthetic RNAs and Dr. Diana Lim for education in the use of Adobe illustrator. We would like to acknowledge the University of Utah Mutation Generation and Detection Core and the Transgenic and Gene Targeting Core for generating the *Bmp4*^{S91C} and *Bmp4*^{E93G} mouse lines. This work utilized DNA and peptide shared resources supported by the Huntsman Cancer Foundation and the National Cancer Institute of the NIH (grant P30CA042014). The content is solely the responsibility of the authors and does not represent the official views of the NIH.

Competing interests

There are no actual or perceived conflicts on the part of any author.

Funding

This work was supported by the Eunice Kennedy Shriver National Institute of Child Health and Human Development, Grant/Award Numbers: R21HD102668; R21HD102668-W1 to JLC; National Institute of Diabetes and Digestive and Kidney Diseases, Grant/Award Number: R01DK128068 to JLC.

Data and resource availability

All relevant data and resource can be found within the article and its supplementary information.

References

Anderson, E. D., Molloy, S. S., Jean, F., Fei, H., Shimamura, S. and Thomas, G. (2002). The ordered and compartment-specfific autoproteolytic removal of the furin intramolecular chaperone is required for enzyme activation. *The Journal of biological chemistry* **277**, 12879-12890.

Aono, A., Hazama, M., Notoya, K., Taketomi, S., Yamasaki, H., Tsukuda, R., Sasaki, S. and Fujisawa, Y. (1995). Potent ectopic bone-inducing activity of bone morphogenetic protein-4/7 heterodimer. *Biochemical and biophysical research communications* **210**, 670-677.

Bakrania, P., Efthymiou, M., Klein, J. C., Salt, A., Bunyan, D. J., Wyatt, A., Ponting, C. P., Martin, A., Williams, S., Lindley, V., et al. (2008). Mutations in BMP4 cause eye, brain, and digit developmental anomalies: overlap between the BMP4 and hedgehog signaling pathways. *Am J Hum Genet* **82**, 304-319.

Bauer, M., Aguilar, G., Wharton, K. A., Matsuda, S. and Affolter, M. (2023). Heterodimerization-dependent secretion of bone morphogenetic proteins in Drosophila. *Developmental cell* **58**, 645-659 e644.

Bonilla-Claudio, M., Wang, J., Bai, Y., Klysik, E., Selever, J. and Martin, J. F. (2012). Bmp signaling regulates a dose-dependent transcriptional program to control facial skeletal development. *Development* **139**, 709-719.

Bragdon, B., Moseychuk, O., Saldanha, S., King, D., Julian, J. and Nohe, A. (2011). Bone morphogenetic proteins: a critical review. *Cellular signalling* **23**, 609-620.

Chauhan, P., Xue, Y., Kim, H. S., Fisher, A. L., Babitt, J. L. and Christian, J. L. (2024). The prodomain of bone morphogenetic protein 2 promotes dimerization and cleavage of BMP6 homodimers and BMP2/6 heterodimers. *The Journal of biological chemistry*, 107790.

Chen, T., Li, Q., Xu, J., Ding, K., Wang, Y., Wang, W., Li, S. and Shen, Y. (2007). Mutation screening of BMP4, BMP7, HOXA4 and HOXB6 genes in Chinese patients with hypospadias. *Eur J Hum Genet* **15**, 23-28.

Chen, X., Zhang, J., Liu, P., Wei, Y., Wang, X., Xiao, J., Wang, C. C. and Wang, L. (2021). Proteolytic processing of secretory pathway kinase Fam20C by site-1 protease promotes biomineralization. *Proceedings of the National Academy of Sciences of the United States of America* **118**.

Constam, D. B. (2014). Regulation of TGFbeta and related signals by precursor processing. *Semin Cell Dev Biol* **32**, 85-97.

Cui, Y., Hackenmiller, R., Berg, L., Jean, F., Nakayama, T., Thomas, G. and Christian, J. L. (2001). The activity and signaling range of mature BMP-4 is regulated by sequential cleavage at two sites within the prodomain of the precursor. *Genes & development* **15**, 2797-2802.

Danesh, S. M., Villasenor, A., Chong, D., Soukup, C. and Cleaver, O. (2009). BMP and BMP receptor expression during murine organogenesis. *Gene expression patterns : GEP* **9**, 255-265.

Degnin, C., Jean, F., Thomas, G. and Christian, J. L. (2004). Cleavages within the prodomain direct intracellular trafficking and degradation of mature bone morphogenetic protein-4. *Molecular biology of the cell* **15**, 5012-5020.

Dunn, N. R., Winnier, G. E., Hargett, L. K., Schrick, J. J., Fogo, A. B. and Hogan, B. L. (1997). Haploinsufficient phenotypes in Bmp4 heterozygous null mice and modification by mutations in Gli3 and Alx4. *Developmental biology* **188**, 235-247.

Durkin, M. E., Qian, X., Popescu, N. C. and Lowy, D. R. (2013). Isolation of Mouse Embryo Fibroblasts. *Bio Protoc* **3**.

Faundes, V., Castillo-Taucher, S., Gonzalez-Hormazabal, P., Chandler, K., Crosby, A. and Chioza, B. (2014). Raine syndrome: an overview. *Eur J Med Genet* **57**, 536-542.

Fujihira, H., Masahara-Negishi, Y., Tamura, M., Huang, C., Harada, Y., Wakana, S., Takakura, D., Kawasaki, N., Taniguchi, N., Kondoh, G., et al. (2017). Lethality of mice bearing a knockout of the Ngly1-gene is partially rescued by the additional deletion of the Engase gene. *PLoS genetics* **13**, e1006696.

Furuta, Y. and Hogan, B. L. (1998). BMP4 is essential for lens induction in the mouse embryo. *Genes & development* **12**, 3764-3775.

Galeone, A., Adams, J. M., Matsuda, S., Presa, M. F., Pandey, A., Han, S. Y., Tachida, Y., Hirayama, H., Vaccari, T., Suzuki, T., et al. (2020). Regulation of BMP4/Dpp retrotranslocation and signaling by deglycosylation. *Elife* **9**.

Galeone, A., Han, S. Y., Huang, C., Hosomi, A., Suzuki, T. and Jafar-Nejad, H. (2017). Tissue-specific regulation of BMP signaling by Drosophila N-glycanase 1. *Elife* **6**.

Goldman, D. C., Donley, N. and Christian, J. L. (2009). Genetic interaction between Bmp2 and Bmp4 reveals shared functions during multiple aspects of mouse organogenesis. *Mechanisms of development* **126**, 117-127.

Goldman, D. C., Hackenmiller, R., Nakayama, T., Sopory, S., Wong, C., Kulessa, H. and Christian, J. L. (2006). Mutation of an upstream cleavage site in the BMP4 prodomain leads to tissue-specific loss of activity. *Development* **133**, 1933-1942.

Gray, A. M. and Mason, A. J. (1990). Requirement for activin A and transforming growth factor--beta 1 pro-regions in homodimer assembly. *Science* **247**, 1328-1330.

Guo, J. and Wu, G. (2012). The signaling and functions of heterodimeric bone morphogenetic proteins. *Cytokine & growth factor reviews* **23**, 61-67.

Harrison, C. A., Al-Musawi, S. L. and Walton, K. L. (2011). Prodomains regulate the synthesis, extracellular localisation and activity of TGF-beta superfamily ligands. *Growth factors* **29**, 174-186.

Jumper, J., Evans, R., Pritzel, A., Green, T., Figurnov, M., Ronneberger, O., Tunyasuvunakool, K., Bates, R., Zidek, A., Potapenko, A., et al. (2021). Highly accurate protein structure prediction with AlphaFold. *Nature* **596**, 583-589.

Kaito, T., Morimoto, T., Mori, Y., Kanayama, S., Makino, T., Takenaka, S., Sakai, Y., Otsuru, S., Yoshioka, Y. and Yoshikawa, H. (2018). BMP-2/7 heterodimer strongly induces bone regeneration in the absence of increased soft tissue inflammation. *Spine J* **18**, 139-146.

Kim, H. S., Neugebauer, J., McKnite, A., Tilak, A. and Christian, J. L. (2019). BMP7 functions predominantly as a heterodimer with BMP2 or BMP4 during mammalian embryogenesis. *Elife* **8**.

Kim, R. Y., Robertson, E. J. and Solloway, M. J. (2001). Bmp6 and Bmp7 are required for cushion formation and septation in the developing mouse heart. *Developmental biology* **235**, 449-466.

Lawson, K. A., Dunn, N. R., Roelen, B. A., Zeinstra, L. M., Davis, A. M., Wright, C. V., Korving, J. P. and Hogan, B. L. (1999). Bmp4 is required for the generation of primordial germ cells in the mouse embryo. *Genes & development* **13**, 424-436.

Lienert, F., Mohn, F., Tiwari, V. K., Baubec, T., Roloff, T. C., Gaidatzis, D., Stadler, M. B. and Schubeler, D. (2011). Genomic prevalence of heterochromatic H3K9me2 and transcription do not discriminate pluripotent from terminally differentiated cells. *PLoS genetics* **7**, e1002090.

Little, S. C. and Mullins, M. C. (2009). Bone morphogenetic protein heterodimers assemble heteromeric type I receptor complexes to pattern the dorsoventral axis. *Nature cell biology* **11**, 637-643.

Liu, C., Zhou, N., Wang, Y., Zhang, H., Jani, P., Wang, X., Lu, Y., Li, N., Xiao, J. and Qin, C. (2018). Abrogation of Fam20c altered cell behaviors and BMP signaling of immortalized dental mesenchymal cells. *Experimental cell research* **363**, 188-195.

Liu, J., Saiyin, W., Xie, X., Mao, L. and Li, L. (2020). Ablation of Fam20c causes amelogenesis imperfecta via inhibiting Smad dependent BMP signaling pathway. *Biol Direct* **15**, 16.

Lubbe, S. J., Pittman, A. M., Matijssen, C., Twiss, P., Olver, B., Lloyd, A., Qureshi, M., Brown, N., Nye, E., Stamp, G., et al. (2011). Evaluation of germline BMP4 mutation as a cause of colorectal cancer. *Hum Mutat* **32**, E1928-1938.

Mimoto, M. S. and Christian, J. L. (2011). Manipulation of gene function in Xenopus laevis. *Methods in molecular biology* **770**, 55-75.

Mimoto, M. S., Kwon, S., Green, Y. S., Goldman, D. and Christian, J. L. (2015). GATA2 regulates Wnt signaling to promote primitive red blood cell fate. *Developmental biology* **407**, 1-11.

Monteiro, R. M., de Sousa Lopes, S. M., Korchynskyi, O., ten Dijke, P. and Mummery, C. L. (2004). Spatio-temporal activation of Smad1 and Smad5 in vivo: monitoring transcriptional activity of Smad proteins. *J Cell Sci* **117**, 4653-4663.

Nakayama, T., Snyder, M. A., Grewal, S. S., Tsuneizumi, K., Tabata, T. and Christian, J. L. (1998). Xenopus Smad8 acts downstream of BMP-4 to modulate its activity during vertebrate embryonic patterning. *Development* **125**, 857-867.

Neugebauer, J. M., Kwon, S., Kim, H. S., Donley, N., Tilak, A., Sopory, S. and Christian, J. L. (2015). The prodomain of BMP4 is necessary and sufficient to generate stable BMP4/7 heterodimers with enhanced bioactivity in vivo. *Proceedings of the National Academy of Sciences of the United States of America* **112**, E2307-2316.

Nixon, T. R. W., Richards, A., Towns, L. K., Fuller, G., Abbs, S., Alexander, P., McNinch, A., Sandford, R. N. and Snead, M. P. (2019). Bone morphogenetic protein 4 (BMP4) loss-of-function variant associated with autosomal dominant Stickler syndrome and renal dysplasia. *Eur J Hum Genet* **27**, 369-377.

Reis, L. M., Tyler, R. C., Schilter, K. F., Abdul-Rahman, O., Innis, J. W., Kozel, B. A., Schneider, A. S., Bardakjian, T. M., Lose, E. J., Martin, D. M., et al. (2011). BMP4 loss-of-function mutations in developmental eye disorders including SHORT syndrome. *Hum Genet* **130**, 495-504.

Schild, R., Knuppel, T., Konrad, M., Bergmann, C., Trautmann, A., Kemper, M. J., Wu, K., Yaklichkin, S., Wang, J., Pestell, R., et al. (2013). Double homozygous missense mutations in DACH1 and BMP4 in a patient with bilateral cystic renal dysplasia. *Nephrol Dial Transplant* **28**, 227-232.

Schwarz, E. (2017). Cystine knot growth factors and their functionally versatile proregions. *Biol Chem* **398**, 1295-1308.

Sengle, G., Ono, R. N., Lyons, K. M., Bachinger, H. P. and Sakai, L. Y. (2008). A new model for growth factor activation: type II receptors compete with the prodomain for BMP-7. *Journal of molecular biology* **381**, 1025-1039.

Shimmi, O., Umulis, D., Othmer, H. and O'Connor, M. B. (2005). Facilitated transport of a Dpp/Scw heterodimer by Sog/Tsg leads to robust patterning of the Drosophila blastoderm embryo. *Cell* **120**, 873-886.

Simpson, M. A., Hsu, R., Keir, L. S., Hao, J., Sivapalan, G., Ernst, L. M., Zackai, E. H., Al-Gazali, L. I., Hulskamp, G., Kingston, H. M., et al. (2007). Mutations in FAM20C are associated with lethal osteosclerotic bone dysplasia (Raine syndrome), highlighting a crucial molecule in bone development. *Am J Hum Genet* **81**, 906-912.

Solloway, M. J. and Robertson, E. J. (1999). Early embryonic lethality in Bmp5;Bmp7 double mutant mice suggests functional redundancy within the 60A subgroup. *Development* **126**, 1753-1768.

Suzuki, S., Marazita, M. L., Cooper, M. E., Miwa, N., Hing, A., Jugessur, A., Natsume, N., Shimozato, K., Ohbayashi, N., Suzuki, Y., et al. (2009). Mutations in BMP4 are associated with subepithelial, microform, and overt cleft lip. *Am J Hum Genet* **84**, 406-411.

Tabatabaeifar, M., Schlingmann, K. P., Litwin, M., Emre, S., Bakkaloglu, A., Mehls, O., Antignac, C., Schaefer, F., Weber, S. and Group, E. T. (2009). Functional analysis of BMP4 mutations identified in pediatric CAKUT patients. *Pediatr Nephrol* **24**, 2361-2368.

Tagliabracci, V. S., Engel, J. L., Wiley, S. E., Xiao, J., Gonzalez, D. J., Nidumanda Appaiah, H., Koller, A., Nizet, V., White, K. E. and Dixon, J. E. (2014). Dynamic regulation of FGF23 by Fam20C phosphorylation, GalNAc-T3 glycosylation, and furin proteolysis. *Proceedings of the National Academy of Sciences of the United States of America* **111**, 5520-5525.

Tagliabracci, V. S., Wiley, S. E., Guo, X., Kinch, L. N., Durrant, E., Wen, J., Xiao, J., Cui, J., Nguyen, K. B., Engel, J. L., et al. (2015). A Single Kinase Generates the Majority of the Secreted Phosphoproteome. *Cell* **161**, 1619-1632.

Thomas, G. (2002). Furin at the cutting edge: from protein traffic to embryogenesis and disease. *Nat Rev Mol Cell Biol* **3**, 753-766.

Tilak, A., Nelsen, S. M., Kim, H. S., Donley, N., McKnite, A., Lee, H. and Christian, J. L. (2014). Simultaneous rather than ordered cleavage of two sites within the BMP4 prodomain leads to loss of ligand in mice. *Development* **141**, 3062-3071.

Uchimura, T., Komatsu, Y., Tanaka, M., McCann, K. L. and Mishina, Y. (2009). Bmp2 and Bmp4 genetically interact to support multiple aspects of mouse development including functional heart development. *Genesis* **47**, 374-384.

Valera, E., Isaacs, M. J., Kawakami, Y., Izpisua Belmonte, J. C. and Choe, S. (2010). BMP-2/6 heterodimer is more effective than BMP-2 or BMP-6 homodimers as inductor of differentiation of human embryonic stem cells. *PloS one* **5**, e11167.

Varadi, M. and Velankar, S. (2023). The impact of AlphaFold Protein Structure Database on the fields of life sciences. *Proteomics* **23**, e2200128.

Wang, X., Fischer, G. and Hyvonen, M. (2016). Structure and activation of pro-activin A. *Nat Commun* **7**, 12052.

Wang, X., Wang, S., Li, C., Gao, T., Liu, Y., Rangiani, A., Sun, Y., Hao, J., George, A., Lu, Y., et al. (2012). Inactivation of a novel FGF23 regulator, FAM20C, leads to hypophosphatemic rickets in mice. *PLoS genetics* **8**, e1002708.

Weber, S., Taylor, J. C., Winyard, P., Baker, K. F., Sullivan-Brown, J., Schild, R., Knuppel, T., Zurowska, A. M., Caldas-Alfonso, A., Litwin, M., et al. (2008). SIX2 and BMP4 mutations associate with anomalous kidney development. *J Am Soc Nephrol* **19**, 891-903.

Wilkinson, D. G. and Nieto, M. A. (1993). Detection of messenger RNA by in situ hybridization to tissue sections and whole mounts. *Methods in enzymology* **225**, 361-373.

Winnier, G., Blessing, M., Labosky, P. A. and Hogan, B. L. (1995). Bone morphogenetic protein-4 is required for mesoderm formation and patterning in the mouse. *Genes & development* **9**, 2105-2116.

Yu, M., Wang, H., Fan, Z., Xie, C., Liu, H., Liu, Y., Han, D., Wong, S. W. and Feng, H. (2019). BMP4 mutations in tooth agenesis and low bone mass. *Arch Oral Biol* **103**, 40-46.

Zhang, H. and Bradley, A. (1996). Mice deficient for BMP2 are nonviable and have defects in amnion/chorion and cardiac development. *Development* **122**, 2977-2986.

Zhang, X., Li, S., Xiao, X., Jia, X., Wang, P., Shen, H., Guo, X. and Zhang, Q. (2009). Mutational screening of 10 genes in Chinese patients with microphthalmia and/or coloboma. *Mol Vis* **15**, 2911-2918.

Zhao, B., Xu, S., Dong, X., Lu, C. and Springer, T. A. (2018). Prodomain-growth factor swapping in the structure of pro-TGF-beta1. *The Journal of biological chemistry* **293**, 1579-1589.

Figure Legends

Figure 1. Point mutations predicted to interfere with phosphorylation of the BMP4 prodomain selectively interfere with BMP4 homodimer but not BMP4/7 heterodimer activity. (A-B) Schematic illustrating sequential cleavage of BMP4 homodimers (A) and BMP4/7 heterodimers (B). (C) Sequence alignment of a portion of the prodomain of human (h), mouse (m), zebrafish (z), *Xenopus* (x) and chick (c) BMP4 to illustrate the conserved S-X-G FAM20C recognition motif. (D) RNA encoding wild type or point mutant forms of BMP4 were injected alone or together with BMP7 near the dorsal marginal zone (DMZ) of 4-cell embryos. DMZ and ventral marginal zone (VMZ) explants were isolated at stage 10 and pSmad1 levels were analyzed by immunoblot as illustrated. Blots were reprobed with actin as a loading control. (E-F) Quantitation of relative pSmad1 levels normalized to actin in at least 3 independent experiments (mean +/- SD, data analyzed using an unpaired t-test). (G) RNA encoding wild type or point mutant forms of BMP4 were injected alone or together with BMP7 near the animal pole of two-cell embryos. Ectodermal explants were isolated at stage 10 and *tbxt* levels were analyzed by semi-quantitative RT-PCR as illustrated. (H-I) Quantitation of relative *tbxt* levels normalized to *odc* in at least 3 independent experiments (mean +/- SD, data analyzed using an unpaired t-test).

Figure 2. $Bmp4^{S91C}$ homozygotes die during mid-embryogenesis and show reduced BMP activity in multiple tissues (A-F) Photograph of E10.5 or E11.5 wild type (A, D) or mutant (B, C, E, F) littermates. Scale bars in Panel A and D apply across each row. (G-J) E10.5 wild type (G, J) or $Bmp4^{S91C/S91C}$ mutant littermates (H, I, K, L) carrying a BRE-LacZ transgene were stained for ß-galactosidase activity to detect endogenous BMP pathway activation. Embryos from a single litter were stained for an identical time under identical conditions. A minimum of three embryos of each genotype were examined and results shown were reproduced in all. G-I show right side and J-L the left side of the same embryos. VPM; ventral posterior mesoderm, BA; branchial arches, SM;

somitic mesoderm. Scale bar corresponds to 1mm in all panels. (M-O) Expression of *Nkx2.5* was analyzed by whole mount in situ hybridization in E10.5 wild type (M) and mutant (N, O) littermates. Photographs of hearts dissected free of embryos are shown. Scale bar in M applies across the row. RA; right atrium, LA; left atrium, RV; right ventricle, LV; left ventricle, OFT; outflow tract.

Figure 3. *Bmp4*$^{-/E93G}$ mutants die during embryogenesis with defects in ventral body wall closure, small or absent eyes and heart defects. (A-G) Photographs of E13.5 (A-C) or E14.5 (D-G) wild type (A, D) or mutant (B, C, E-G) littermates. The position of the liver inside (A-E, F) or outside (C, G) of the abdomen is indicated. (H, I) Hematoxylin and eosin stained coronal sections of hearts dissected from E14.5 wild type (H) or *Bmp4*$^{-/E93G}$ littermates (I). Asterisk denotes VSD and arrowheads indicate thin, non-compacted ventricular wall (I). Scale bar applies across each row.

Fig. 4. E93G and S91C mutations lead to accumulation of BMP4 precursor protein and reduced levels of cleaved ligand and pSmad1 in vivo. (A-H) Levels of pSmad1 and BMP4 were analyzed in protein lysates isolated from E10.5 *Bmp4*^{S91C} (A-D) or *Bmp4*^{E93G} (E-H) homozygotes, heterozygotes or wild type littermates. (I-P) Levels of pSmad1, BMP4 precursor protein and cleaved BMP4 ligand were analyzed in cell lysates and conditioned media of MEFs isolated from E13.5 *Bmp4*^{S91C} heterozygotes or wild type littermates (I-L) or from *Bmp4*^{E93G} homozygotes, heterozygotes or wild type littermates (M-P). Representative blots (A, E, I, K) and quantitation of protein levels normalized to actin (mean +/- SD, data analyzed using an unpaired t-test) (B-D, F-H, J-L, N-O) are shown.

Fig. 5. BMP4^{E93G} and BMP4^{S91C} precursor proteins are O-glycosylated and exit the ER. (A, B) MEFs were isolated from E13.5 *Bmp4*^{S91C} heterozygotes, *Bmp4*^{E93G} homozygotes, or wild type littermates.Protein lysates were left untreated or were treated with O-glycosidase and α-

neuraminidase to remove O-linked glycosylation (A) or with EndoH or PNGase to remove N-linked glycosylation (B). Immunoblots were probed with antibodies directed against BMP4 to detect BMP4 precursor protein. Bands corresponding to Endo H-sensitive (asterisks) and Endo H-resistant PNGase-sensitive BMP4 (arrowheads) are indicated in B.

Fig. 6. Hypothetical models for how prodomain phosphorylation regulates proteolytic maturation of BMP4. (A) Model 1: Phosphorylation of BMP4 by Fam20C within the TGN directs subcellular trafficking of BMP4 out of the golgi to the cell surface via a route that is distinct from the pathway taken by furin. Furin- and BMP4-containing vesicles fuse in a region adjacent to the cell surface where furin cleaves BMP4 to release the active ligand. (B) Model 2: Fam20C, BMP4 and furin traffic together to a membrane proximal subcellular compartment where Fam20C becomes catalytically activated (lightening bolt) and phosphorylates the prodomain of BMP4. Phosphorylation enables furin to access and cleave the consensus motif on BMP4. (C) Structure of BMP4 precursor monomer predicted by alphafold. N-terminus in blue, C-terminus in red. Boxed region includes Ser91 and the furin consensus motif. (D-E) Close up of boxed region in C illustrating the close proximity between Ser91 (pink letters) within the prodomain in its unphosphorylated (D) or phosphorylated (E) form and the -R^{287}-R-R-A-K-R^{292} furin consensus motif at the C-terminus of the prodomain. Red arrows indicate the site of furin cleavage. (F-G) Spacefill representation of the of the structures of BMP4 precursor protein homodimers (F) or BMP4 (light gray) and BMP7 (dark gray) precursor protein heterodimers (G) predicted by alphafold with the location of furin recognition motifs denoted in purple.

Table 1. Progeny from *Bmp4*$^{S91C/+}$ or *Bmp4*$^{E93G/+}$ intercrosses, or from *Bmp4*$^{-/+}$ and *Bmp4*$^{E93G/+}$ intercrosses at P28.

A. Progeny from *Bmp4*$^{S91C/+}$ intercrosses at P28

Sex	*Bmp4*$^{+/+}$	*Bmp4*$^{S91C/+}$	*Bmp4*$^{S91C/S91C}$	*n*	*p*
Both	12 (21%)	44 (79%)	0 (0%)	56	0.00001
Male	7 (23%)	23 (77%)	0 (0%)	30	0.0027
Female	6 (23%)	20 (77%)	0 (0%)	26	0.0034

Data are presented as number (percent).

B. Progeny from *Bmp4*$^{E93G/+}$ intercrosses at P28

Sex	*Bmp4*$^{+/+}$	*Bmp4*$^{E9G3G/+}$	*Bmp4*$^{E93G/E93G}$	*n*	*p*
Both	35 (28%)	74 (59%)	16 (13%)	125	0.007
Male	19 (31%)	31 (50%)	12 19%)	62	0.454
Female	17 (27%)	44 (70%)	4 (6%)	63	0.002

Data are presented as number (percent).

C. Progeny from *Bmp4*$^{-/+}$ x *Bmp4*$^{E93G/+}$ at P28

Sex	*Bmp4*$^{+/+}$	*Bmp4*$^{E9G3G/+}$	*Bmp4*$^{-/+}$	*Bmp4*^{E93G}	*n*	*p*
Both	22 (36%)	22 (36%)	17 (28%)	0 (0%)	61	0.0001
Male	10 (33%)	9 (30%)	11 (37%	0 (0%)	30	0.0164
Female	13 (42%)	11 (35%)	7 (23%)	0 (0%)	31	0.0052

Data are presented as number (percent).

D. Progeny from *Bmp4*$^{S91C/+}$ x *Bmp4*$^{E93G/+}$ at P28

Sex	*Bmp4*$^{+/+}$	**Bmp4*$^{S91C/+}$ or *Bmp4*^{E9G3}	*Bmp4*$^{ES91C/E93}$	*n*	*p*
Both	23 (33%)	39 (56%)	7 (11%)	69	0.014
Male	9 (25%)	23 (64%)	4 (11%)	36	0.125
Female	14 (42%)	16 (48%)	3 (9%)	33	0.025

Data are presented as number (percent).

*Genotyping protocol does not distinguish between *Bmp4*$^{S91C/+}$ or *Bmp4*$^{E9G3G/+}$ allele and thus heterozygotes are pooled.

Table 2. Progeny from *Bmp4*$^{S91C/+}$ intercrosses, or from *Bmp4*$^{-/+}$ and *Bmp4*$^{E93G/+}$ Intercrosses at embryonic ages.

A. Progeny from *Bmp4*$^{S91C/+}$ inter se crosses

Age	*Bmp4*$^{+/+}$	*Bmp4*$^{S91C/+}$	*Bmp4*$^{S91C/S91C}$	*n*	*p*
E13.5	22 (29%)	55 (71%)	0 (0%)	77	0.00001
E11.5	21 (37%)	35 (63%)	0 (0%)	56	0.0002
E10.5	43 (21%)	18 (58%)	43 (21%)	204	0.2110
E9.5	7 (14%)	31 (66%)	9 (19%)	47	0.0838

Data are presented as number (percent).

B. Progeny from *Bmp4*$^{E93G/+}$ x *Bmp4*$^{-/+}$ crosses

Age	*Bmp4*$^{+/+}$	*Bmp4*$^{E93G/+}$	*Bmp4* $^{-/+}$	*Bmp4*$^{-/E93G}$	*n*	*p*
E13.5-14.5	17 (26%)	13 (19%)	19 (29%)	17 (26%)	66	0.765
E11.5-12.5	11 (27%)	4 (10%)	12 (29%)	14 (34%)	41	0.136
E10.5	7 (24%)	10 (35%)	7 (24%)	5 (17%)	29	0.624

Data are presented as number (percent).

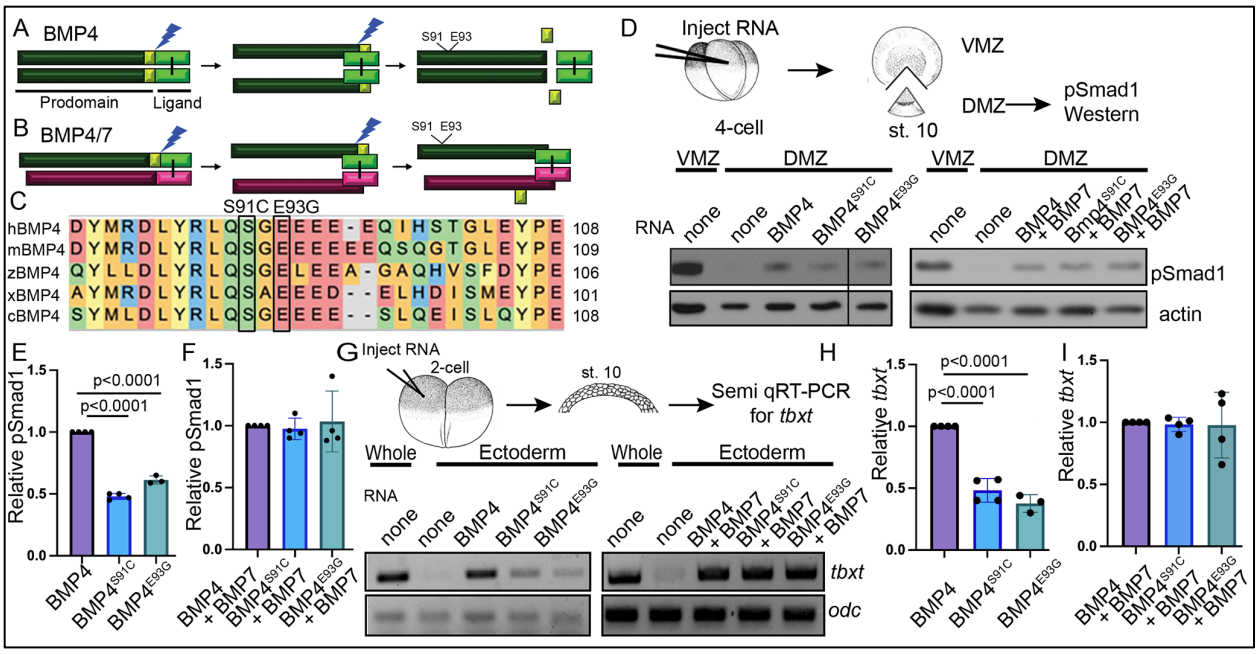

Figure 1. Point mutations predicted to interfere with phosphorylation of the BMP4 prodomain selectively interfere with BMP4 homodimer but not BMP4/7 heterodimer activity.

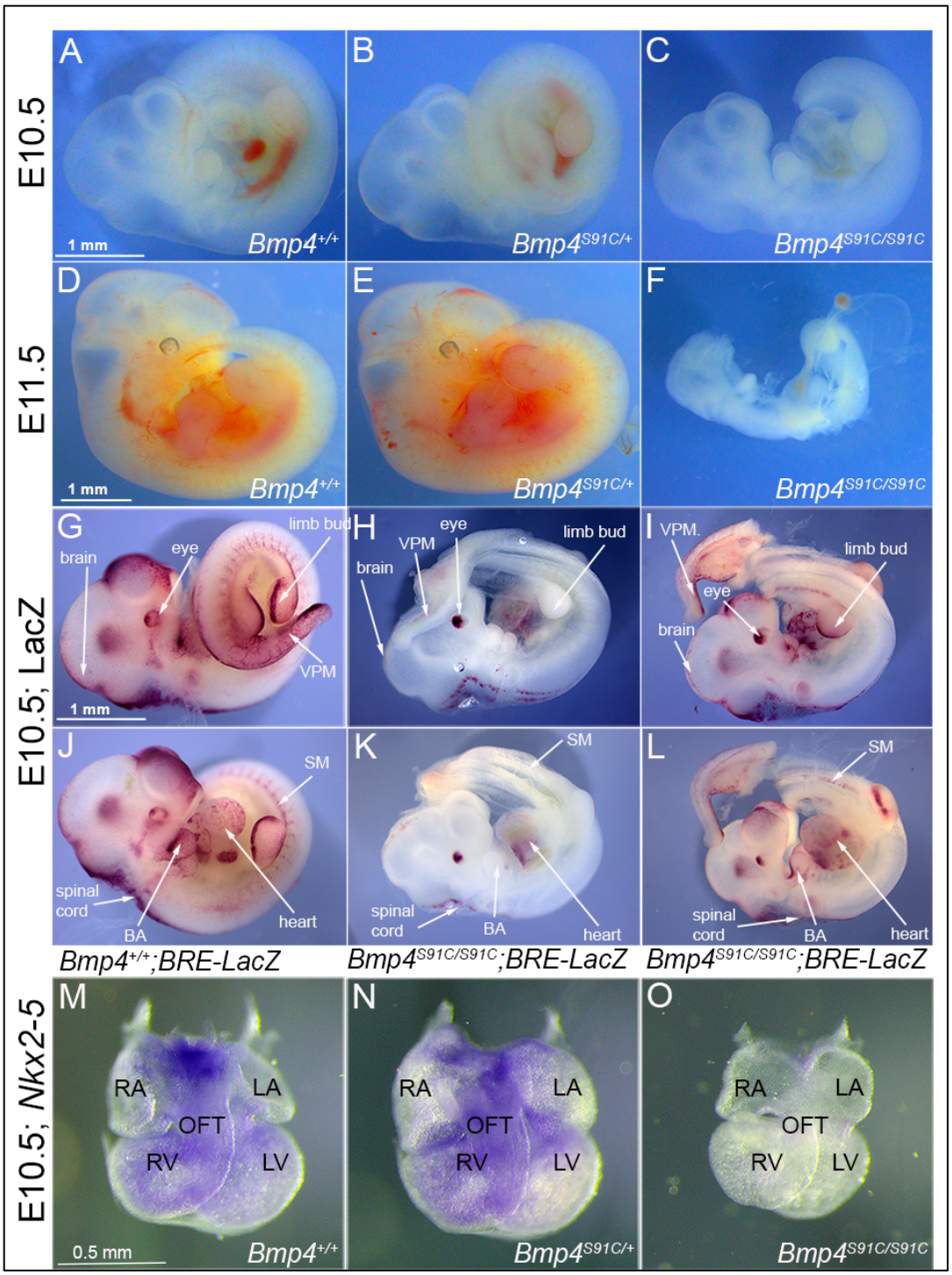

Figure 2. Bmp4^{S91C} homozygotes die during mid-embryogenesis and show reduced BMP activity in multiple tissues.

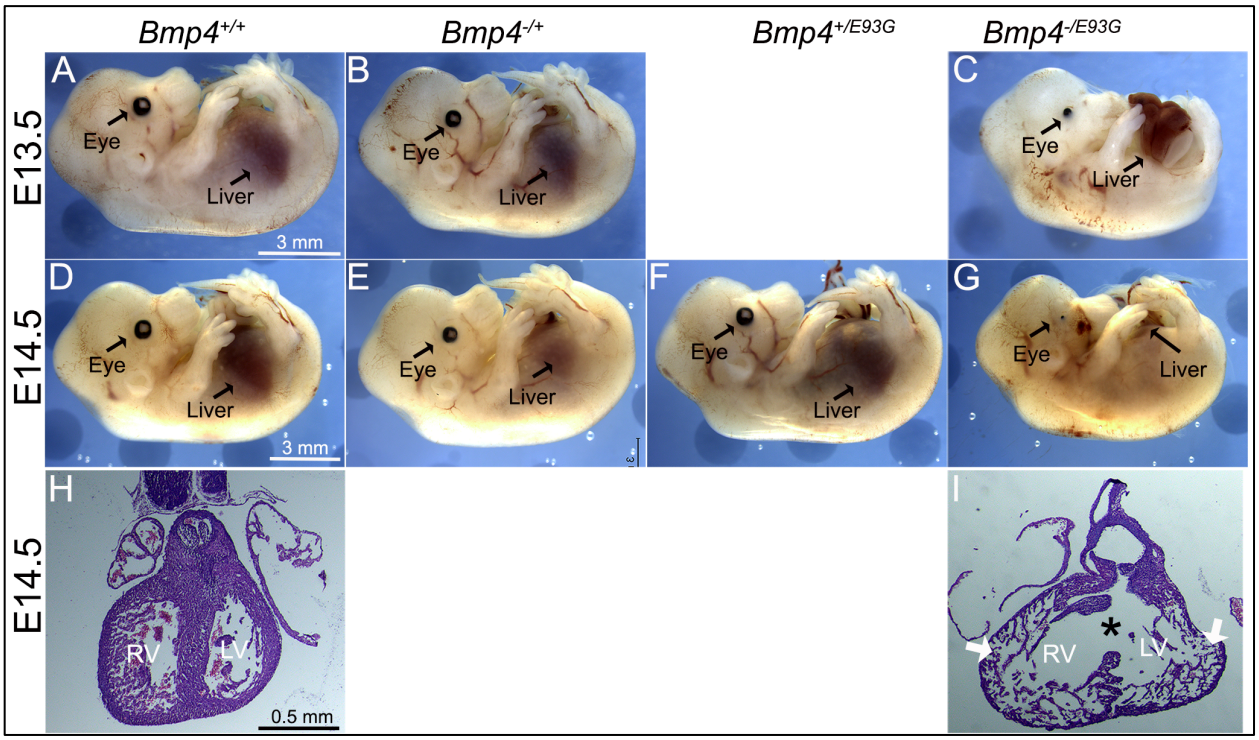

Figure 3. *Bmp4*$^{-/E93G}$ mutants die during embryogenesis with defects in ventral body wall closure, small or absent eyes and heart defects.

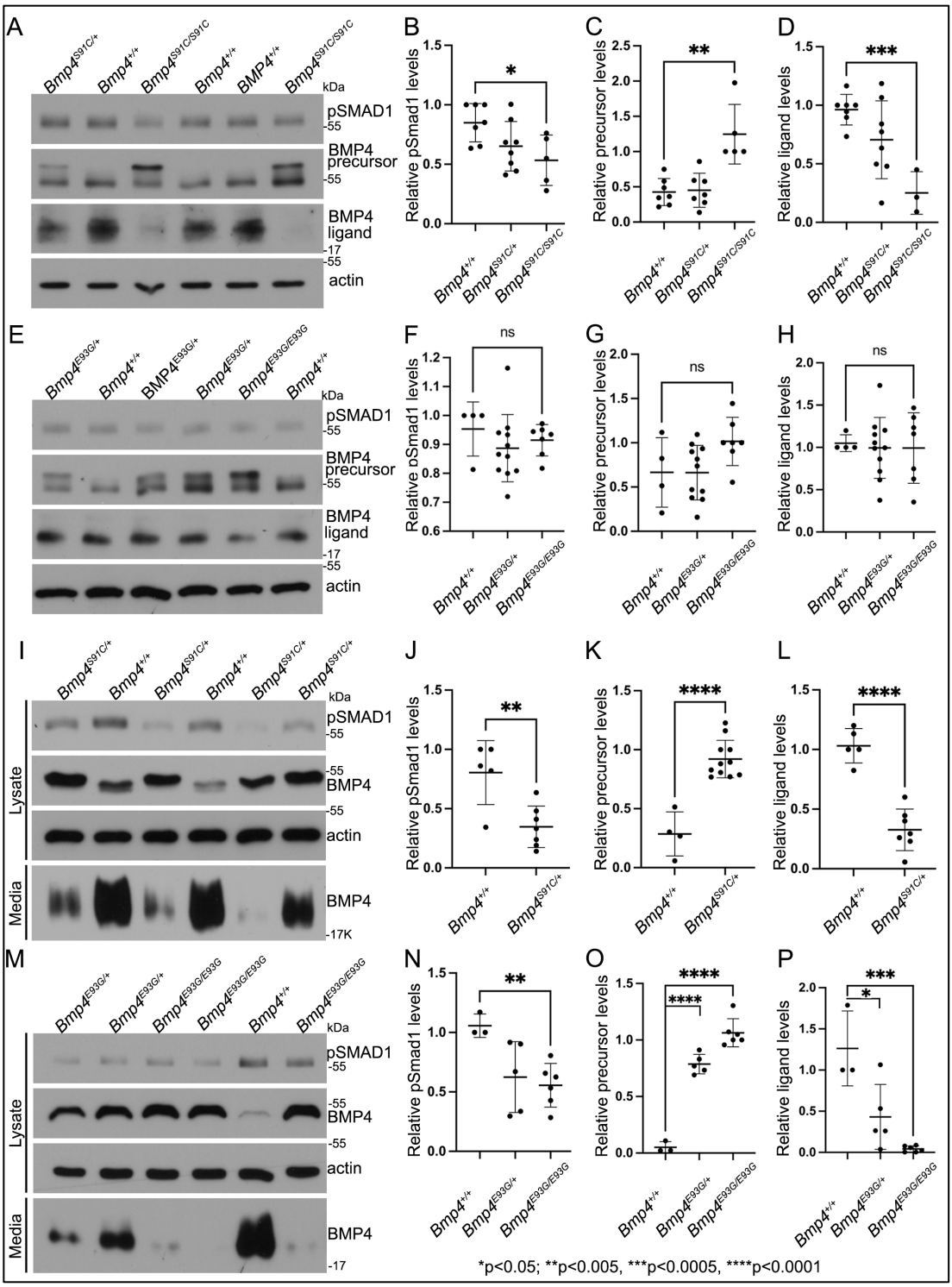

Fig. 4. p.E93G and p.S91C mutations lead to accumulation of BMP4 precursor protein and reduced levels of cleaved ligand and pSMAD1 in vivo.

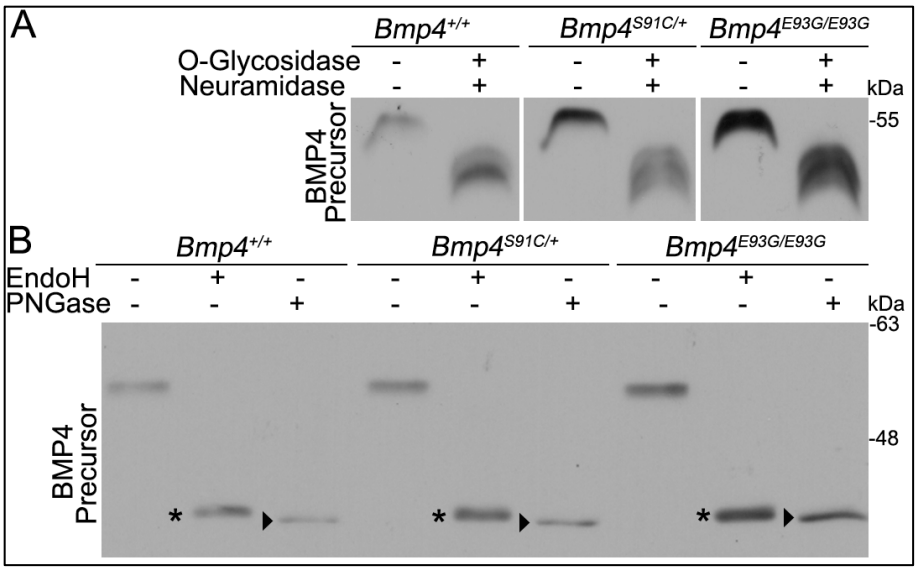

Fig. 5. BMP4^{E93G} and BMP4^{S91C} precursor proteins are O-glycosylated and exit the ER.

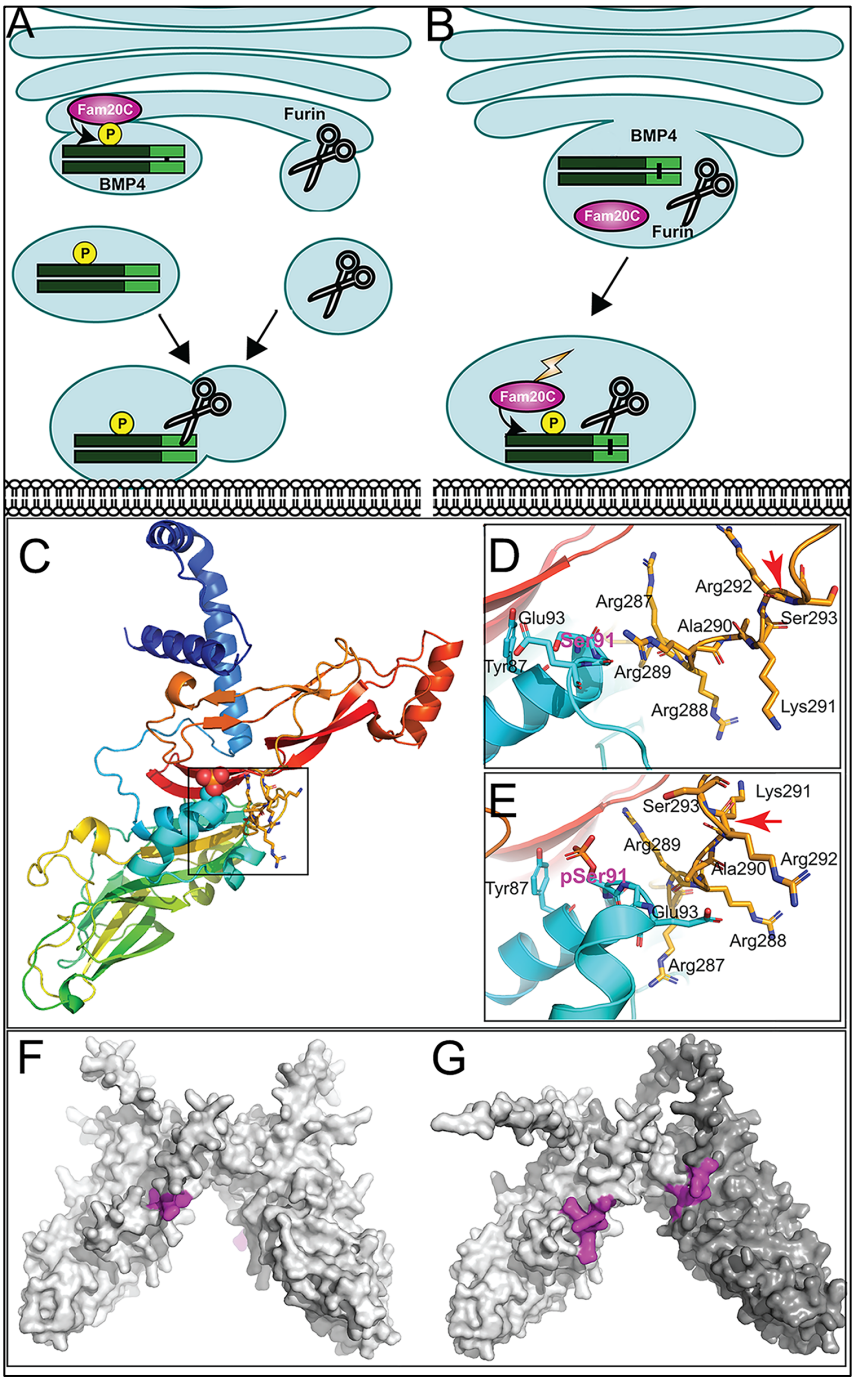

Fig. 6. Hypothetical models for how prodomain phosphorylation facilitates proteolytic maturation of BMP4.